Radiation Protection Dosimetry (2005) Vol. 113, No. 1, pp. 75–89
Advance Access publication 30 November 2004
doi:10.1093/rpd/nch423

ANALYSIS OF A KALMAN FILTER BASED METHOD FOR ON-LINE ESTIMATION OF ATMOSPHERIC DISPERSION PARAMETERS USING RADIATION MONITORING DATA

Martin Drews[1,2], Bent Lauritzen[1,*] and Henrik Madsen[2]
[1]Risø National Laboratory, DK-4000 Roskilde, Denmark
[2]Informatics and Mathematical Modelling, Technical University of Denmark, DK-2800 Kgs. Lyngby, Denmark

Received June 14 2004, amended October 18 2004, accepted October 26 2004

A Kalman filter method is discussed for on-line estimation of radioactive release and atmospheric dispersion from a time series of off-site radiation monitoring data. The method is based on a state space approach, where a stochastic system equation describes the dynamics of the plume model parameters, and the observables are linked to the state variables through a static measurement equation. The method is analysed for three simple state space models using experimental data obtained at a nuclear research reactor. Compared to direct measurements of the atmospheric dispersion, the Kalman filter estimates are found to agree well with the measured parameters, provided that the radiation measurements are spread out in the cross-wind direction. For less optimal detector placement it proves difficult to distinguish variations in the source term and plume height; yet the Kalman filter yields consistent parameter estimates with large associated uncertainties. Improved source term assessment results, when independent estimates of the plume height can be used. Perspectives for using the method in the context of nuclear emergency management are discussed, and possible extensions to the present modelling scheme are outlined, to account for realistic accident scenarios.

INTRODUCTION

Recently, a Kalman filter method was proposed as a means for on-line parameter estimation in the gaussian plume model using off-site radiation monitoring data[(1)]. In the state space model formalism, the temporal variations of the plume model parameters, treated as state variables, are described by a stochastic dynamic equation, while a static measurement equation relates the state variables to the observables, for example, environmental gamma dose or fluence rates. The Kalman filter is essentially a sequential predictor–corrector algorithm, where the model forecasts are recursively updated by weighting the difference between the predicted model output and the observations by an optimal gain factor, that is, by exercising a sort of feedback control. The embedded parameters of the state space model are determined from the data by maximum likelihood estimation, making the approach almost free of external parameters.

Using simulated data, the proposed method was found to provide stable and reliable estimates of the plume model parameters and their associated uncertainty as well as of the embedded parameters of the state space model. Preliminary studies based on data from an ^{41}Ar atmospheric dispersion experiment carried out at a nuclear research reactor in Mol, Belgium[(2)] further indicate that the method could be an efficient operational tool for source term estimation following a nuclear accident.

In the present paper, we test the Kalman filter method more thoroughly on the entire data set from the ^{41}Ar atmospheric dispersion experiment. Three different state space models are examined, differing in the number of unknown parameters. For the two simplest models, the dynamics of a subset of the gaussian plume model parameters are governed by a random walk process, while the remaining parameters are set externally. In the third, more elaborate model, we allow for spatial variation in the wind field to account for differences between the plume advection direction and the observed wind direction. The three different models are compared with respect to their ability to estimate the source term and plume geometry observed in the experiment. Finally, possible extensions to the simple state space models are discussed, as well as the perspectives of using the method in decision support systems for nuclear emergency management.

METHOD

In the state space model the atmospheric dispersion parameters, for example, the source term and plume advection direction, are treated as stochastic state variables. Denoting the m state variables at time t by $x_{i,t}; i = 1, \ldots, m$, the time evolution of the state $X_t^{\mathrm{T}} = (x_{1,t}, x_{2,t}, \ldots, x_{m,t})$ is governed by the

*Corresponding author: bent.lauritzen@risoe.dk

stochastic system equation,

$$X_t = f(X_{t-1}, u_t) + w_t, \tag{1}$$

while the physical observables, $Y_t^{\mathrm{T}} = (y_{1,t}, y_{2,t}, \ldots, y_{n,t})$, are linked to the state variables through the static measurement equation,

$$Y_t = h(X_t) + v_t. \tag{2}$$

In the above equations, f describes the dynamics of the state variables, where u_t is an optional forcing term, h is the atmospheric dispersion model relating the observables (e.g. dose rate) to the state variables, and w_t and v_t denote stochastic noise processes, the latter accommodating both dispersion model uncertainty and measurement error. Here, we will assume w_t and v_t to be uncorrelated white noise gaussian processes with zero mean and covariance matrices Q_t and R_t, respectively.

The estimator of the state at a time t, $\hat{X}_{t|s}$, given all observations up to and including time s is provided by the generalised discrete Kalman filter equations[3–5], comprising *a priori* state estimates (time updates, $s = t-1$) and *a posteriori* state estimates (measurement updates, $s = t$), that is,

- Time update:

$$\hat{X}_{t|t-1} = f\left(\hat{X}_{t-1|t-1}, u_t\right), \tag{3}$$

$$\Sigma^{xx}_{t|t-1} = A_t \Sigma^{xx}_{t-1|t-1} A_t^{\mathrm{T}} + Q_t. \tag{4}$$

- Measurement update:

$$K_t = \Sigma^{xx}_{t|t-1} H_t^{\mathrm{T}} \left(H_t \Sigma^{xx}_{t|t-1} H_t^{\mathrm{T}} + R_t\right)^{-1}, \tag{5}$$

$$\hat{X}_{t|t} = \hat{X}_{t|t-1} + K_t\left(Y_t - h\left(\hat{X}_{t|t-1}\right)\right), \tag{6}$$

$$\Sigma^{xx}_{t|t} = \Sigma^{xx}_{t|t-1} - K_t H_t \Sigma^{xx}_{t|t-1}, \tag{7}$$

were $\Sigma^{xx}_{t|s} \equiv V[X_t | Y_s, Y_{s-1}, \ldots, Y_1]$ is the state error covariance based on all observations up to and including time s. The matrices A_t and H_t are the partial derivatives of f and h with respect to the state variables,

$$(A_t)_{ij} = \frac{\partial f_i}{\partial x_j}\left(\hat{X}_{t-1|t-1}, u_t\right), \tag{8}$$

$$(H_t)_{ij} = \frac{\partial h_i}{\partial x_j}\left(\hat{X}_{t|t-1}\right), \tag{9}$$

resulting from linearising the system and measurement equations around the current state estimate. To initialise the Kalman filter one must define the initial state estimates $(\hat{X}_{0|0}, \Sigma^{xx}_{0|0})$. These parameters along with other embedded parameters of the state space model, for example, the system and measurement error covariance matrices Q_t and R_t, may be set externally or estimated from the observations. Finally, it is assumed that the state space model is observable[5], that is, that an estimate of the state vector X_t can be obtained from the measurements Y_t.

The precision of the state estimates is determined by the system and measurement error covariance matrices, Q_t and R_t, embedded in the state space model. Rather than relying on subjectively selected parameters, the set of unknown state space parameters $\beta = \{Q_t, R_t, \hat{X}_{0|0}, \Sigma^{xx}_{0|0}, \ldots\}$ may be determined by maximum likelihood estimation[1]. Based on N observations of the measurement vector, $\Omega_N = \{Y_N, \ldots, Y_1\}$, the log-likelihood function is given by

$$\ln L(\beta; \Omega_N) = -\frac{1}{2}\sum_{t=1}^{N}\Big\{\ln \det \Sigma^{yy}_{t|t-1} + \varepsilon_t^{\mathrm{T}}\left(\Sigma^{yy}_{t|t-1}\right)^{-1}\varepsilon_t\Big\} + \text{const.} \tag{10}$$

The term $\varepsilon_t = Y_t - h\left(\hat{X}_{t|t-1}\right)$ is the innovation, which is provided by the Kalman filter along with the associated covariance $\Sigma^{yy}_{t|t-1} = H_t \Sigma^{xx}_{t|t-1} H_t^T + R_t$, cf. Equations 5 and 6. The maximisation of the log-likelihood function (10) must, in general, be carried out using non-linear numerical optimisation[6,7].

The observables Y_t consist of simultaneous measurements of the radiation field, for example, environmental dose rates or as in the present study primary photon fluence rates, φ, along with observations of the wind direction, θ^{w}, from a weather mast. Hence, the model for the observables, $Y_t = h(X_t) + v_t$, is given by

$$h^{\mathrm{T}} = (\varphi_1, \ldots, \varphi_{n-1}, \theta^{\mathrm{w}}). \tag{11}$$

The fluence rate at a detector position, $\vec{r}_k$, is calculated from the general expression,

$$\varphi(\vec{r}_k) = \frac{1}{4\pi}\int \mathrm{d}^3\vec{r}\ \frac{\chi(\vec{r})\exp(-\mu|\vec{r} - \vec{r}_k|)}{(\vec{r} - \vec{r}_k)^2} y_\gamma, \tag{12}$$

where $\chi(\vec{r})$ is the radionuclide activity concentration, μ is the linear attenuation coefficient and the photon yield y_γ is the number of photons per disintegration.

In the gaussian plume model the activity concentration is written as

$$\chi(\vec{r}) = \frac{\theta(x)\dot{Q}}{2\pi u \sigma_y(x)\sigma_z(x)} \exp\left(-\frac{y^2}{2\sigma_y^2(x)}\right) \times \left\{\exp\left(-\frac{(z-h)^2}{2\sigma_z^2(x)}\right) + \exp\left(-\frac{(z+h)^2}{2\sigma_z^2(x)}\right)\right\}, \quad (13)$$

where, x denotes the downwind distance from the release point along the plume advection direction θ (the plume centreline), y is the cross-wind distance and z the height above the ground. $\dot{Q}$ is the radionuclide emission rate, u the wind speed and h is the effective plume height, while $\sigma_y(x)$ and $\sigma_z(x)$ are the horizontal and vertical plume dispersion parameters in the y- and z-direction, respectively. The term $\theta(x)$ denotes the Heaviside unit function, restricting the activity concentration to the region $x > 0$. The model prediction for the wind direction is obtained by equating the observed wind direction to the plume advection direction, $\theta_t^w = \theta_t$.

In the present study, we restrict ourselves to a linear stochastic system equation, that is,

$$X_t = AX_{t-1} + u_t + w_t. \quad (14)$$

The state variables $X_t^{\mathrm{T}} = \left(\dot{Q}/u, h, \theta, \sigma_y, \sigma_z\right)_t$ are the parameters of the gaussian plume model. Since in the model we cannot distinguish variations in the emission rate from variations in the wind speed without independent measurements of either of these quantities, we will, henceforth, refer to the ratio $\dot{Q}/u$ as the source term. Furthermore, the unknown system and measurement error covariance matrices Q_t and R_t embedded in the state space model (1) and (2) are assumed to be constant and diagonal. To account for missing observations, however, the corresponding matrix elements of R_t are assigned infinite values. In the evaluation of Equations 12 and 13, we use a numerically efficient implementation based on an approximate one-dimensional integral solution[1,8].

EXPERIMENTAL DATA

The Kalman filter method is applied to a set of radiation monitoring data, which were obtained during 3–5 October 2001 at the BR1 research reactor at the Belgium Nuclear Research Center (SCK•CEN) in Mol[2,9]. The experiment was carried out as part of the Nordic Nuclear Research project NKS/BOK-1[10] and in collaboration with SCK•CEN. Using an array of gamma detectors, ground level measurements of the radiation field owing to gamma decay of ^{41}Ar (E_γ = 1293.6 keV, y_γ = 0.992) released from the 60-m emission stack were performed over a period of 3 d along with measurements of all the essential meteorological parameters (e.g. wind direction and speed) from the on-site weather mast. Continuous measurements of the source term were obtained by extracting air samples from the emission stack and measuring the activity concentration using a plastic scintillator. During the experiment, the reactor thermal power was kept constant at 700 kW and the atmospheric air from the air-cooled reactor ventilated at a rate of $\sim$9.4 m^3 s^{-1}, giving rise to a relatively constant ^{41}Ar emission rate. Direct measurements of the plume geometry were performed by injecting a white aerosol tracer into the cooling air stream from the reactor, which was subsequently scanned using a Lidar technique based on a pulsed laser beam[11,12]. From the Lidar scans, plume aerosol cross-section profiles were obtained in addition to the horizontal and vertical plume centreline position.

During the experiment, four gamma detectors labelled A–D were set up to span the plume based on 6-h forecasts for the wind direction, taking into account the terrain requirements. The four detectors are identical, thermally insulated NaI(Tl) detectors and provide 512-channel spectra every 30 s from which background corrected measurements of the primary photon fluence rate are obtained. For the purpose of this study, the spectral counts are binned in synchronised 1-min intervals. Four time series were recorded during the experiment. Schematical drawings of the detector positions and the mean wind direction are shown in Figure 1; the corresponding time series are summarised in Table 1. Since the weather mast was located several hundred metres away from the gamma detectors, measurements of the wind direction may deviate from the main plume advection direction.

Note that the data from 4 October, which was obtained over a full day of reactor operation, is split into two separate data sets of roughly equal length (Series 2 and 3). Since the detectors were occasionally recalibrated to account for thermal drift in the recorded energy spectra, missing measurements occur in all time series for one or more of the detectors.

NUMERICAL RESULTS

Initially, we consider two different state space models, differing only in the treatment of the plume height. In Model I, the unknown plume parameters are the source term, the plume height and the main advection direction, that is, $X_t^{\mathrm{T}} = \left(\dot{Q}/u, h, \theta\right)_t$, while in Model II the state vector is $X_t^{\mathrm{T}} = \left(\dot{Q}/u, \theta\right)_t$, cf.

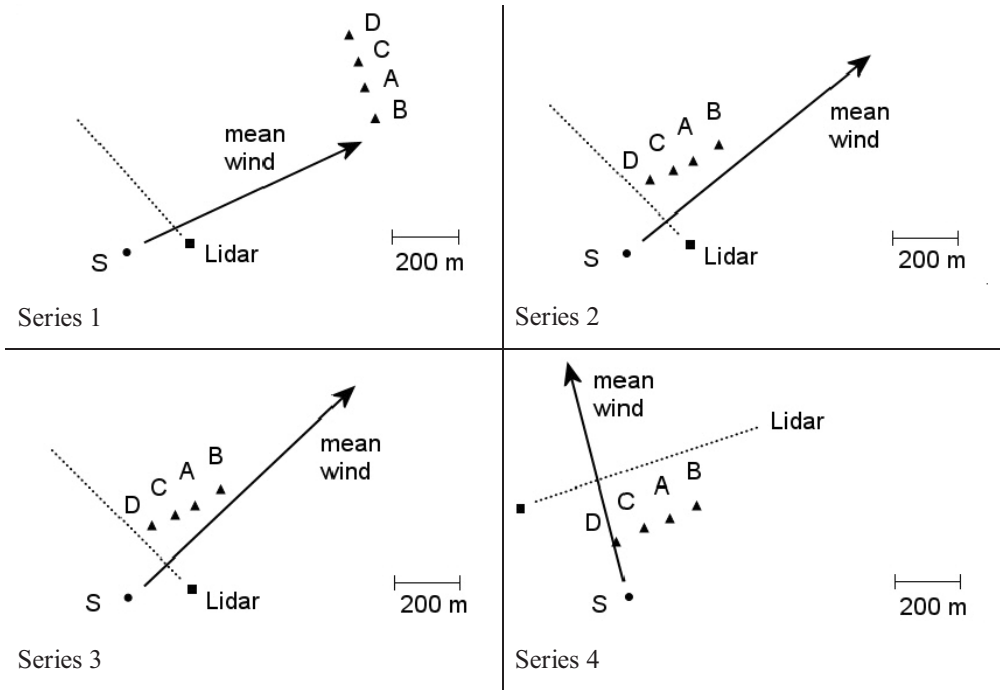

Figure 1. The detector set-up (A–D) of the four time series, cf. Table 1. 'S' is the emission stack and the mean wind direction is shown for each of the time series. The Lidar scanning directions are indicated by dotted lines.

Table 1. Data sets.

Data set	# measurements (min)	Period
Series 1	90	3 Oct. at 15.36–17.05
Series 2	166	4 Oct. at 11.43–14.28
Series 3	175	4 Oct. at 14.29–17.23
Series 4	123	5 Oct. at 09.53–11.55

Table 2. State space models.

	Free parameters	External parameters
Model I	$\dot{Q}/u, h, \theta$	σ_y, σ_z
Model II	$\dot{Q}/u, \theta$	h, σ_y, σ_z

Table 2. In case of an accidental airborne release, little or no information may be available on the plume height, which is an important parameter, especially for long-distance transport. This is accounted for in Model I, where the plume height is a free parameter to be determined through the Kalman filter. In Model II, the availability of independent and reliable estimates of the plume height is assumed. The plume height is here set externally as a forcing term $h_t = h_t^u$, based on the theoretical formulae for buoyant plume rise by Briggs[13]. Similarly, in both models σ_y and σ_z are set externally using a site-specific parameterisation of the dispersion parameters[14], for example, $\sigma_{y,t} = \sigma_{y,t}^u$, that depends on the distance from the source and the atmospheric stability according to the Pasquill–Gifford scheme[15]. A simple random walk process is used to govern the temporal variations of the remaining (free) state variables, cf. Equation 14,

$$x_{i,t} = x_{i,t-1} + w_{i,t}. \tag{15}$$

The observables Y_t are the gamma fluence rates recorded by the four detectors and the instantaneous wind direction measured from the weather mast.

Figure 2 shows the Kalman filter predictions $\hat{Y}_{t|t-1} = h(\hat{X}_{t|t-1})$ for Model I and Series 1. The Kalman filter is seen to provide a smooth fit to the experimental data. The fluence rate predictions systematically lag one time-step behind the measurements as would be expected from the current model and Equation 3, while the measured wind direction display more irregular deviations from the prediction. This is expected since the plume advection direction is an average over the transit from source to the detectors. Similar results were obtained for the other three time series. From the Kalman filter, estimates of

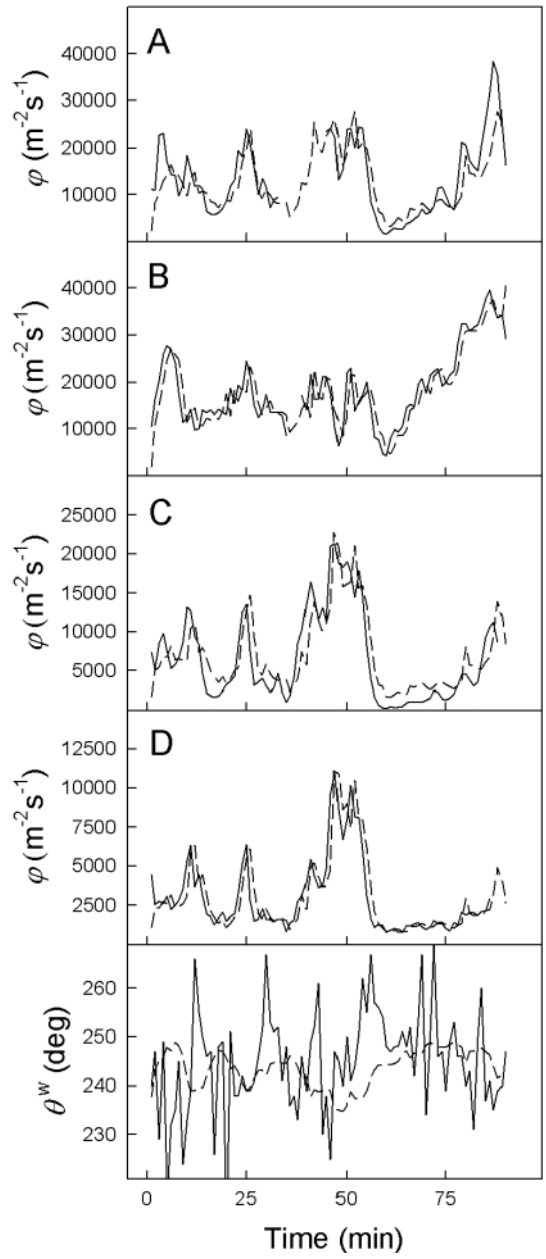

Figure 2. Kalman filter predictions $\hat{Y}_{t|t-1} = h(\hat{X}_{t|t-1})$ for Model I and Series 1 (dashed lines). The full lines are the measured values, Y_t.

the unobserved fluence rates are obtained based on the remaining available information, for example, for detector A in the interval 34–44 min (top panel).

Figures 3–6 show the *a posteriori* Kalman filter estimates of the plume model parameters, $\hat{X}_{t|t}$, and the associated standard errors obtained from the covariance matrix $\Sigma^{xx}_{t|t}$ for Models I and II for all the time series. Also shown are the direct observations of the source term, plume height and wind direction, as well as the theoretical height including plume rise.

For Series 1 (Figure 3), Model I predicts a source term that is up to four times larger than the measured value and a plume height that is up to twice that of the theoretical predictions. Since the Lidar in this experiment was placed far away from the detector line (Figure 1), yielding only an inaccurate estimate of the height, no direct measurements of the plume height are available for this data set. The seeming overestimation of both source term and plume height is most probably caused by the strong correlation between the source term and the plume height, giving rise to a state identification problem. To resolve the variations in these parameters using ground level radiation measurements only, the detectors must be spread out sufficiently in the cross-wind direction[1]. For Series 1 the estimated horizontal plume dispersion parameter, σ_y, is of the order of 100 m at the location of the detectors. The width of the plume is thus comparable to the region covered by the detectors (Figure 1), and the spatial separation of the detectors is not sufficient to resolve variations in the plume height and source term.

For Series 2 and 3 the detectors are placed almost parallel to the mean wind direction and close to the plume centreline (Figure 1). For Series 2 (Figure 4), Model I wrongly indicates a near ground-level plume with the estimated standard deviation being of the same order of magnitude as the predicted height, while Lidar measurements as well as the theoretical plume height is close to or exceeding the height of the emission stack. Slightly better results for the plume height are obtained for Series 3 (Figure 5). The estimated plume height is here seen to coincide better with the measurements but to exhibit fast fluctuations, suggesting numerical instability. The fluctuations are mirrored in the estimated standard deviations. In both cases, Model I estimates the source term to exceed the measurements by up to a factor of two.

For Series 4 (Figure 6) the detectors are placed perpendicular to the plume centreline, and the estimated plume height agrees well with the measured height. Likewise, the source term estimates agree well with the measurements, in particular during the first 50 min of the time series. Thus the Kalman filter seems to be able to resolve the variations in source term and plume height correctly. The peaks observed in the estimated standard deviations at 90 min are caused by all the gamma detectors simultaneously being off-line and hence no radiation data being available to correct the Kalman filter predictions. As new measurements become available, the variance estimates for all parameters quickly drops to a lower value.

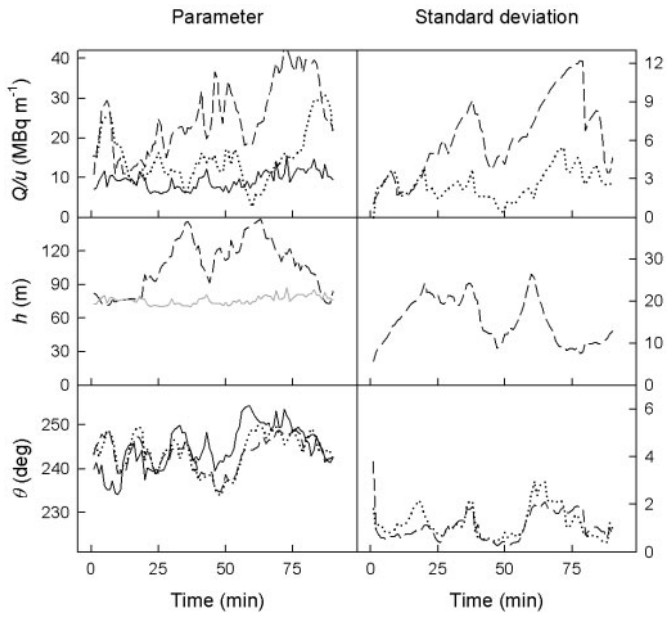

Figure 3. Model parameters and associated standard deviations for Series 1. The dashed and dotted curves are the *a posteriori* parameter estimates using Models I and II, respectively, while the solid curves are the experimental data. The solid grey line in the middle left panel is the theoretical plume height calculated according to Briggs[13]. The wind direction measurements shown in the lower left panel have been exponentially smoothened (smoothing constant = 0.2)[4] to reduce rapid fluctuations associated with the frequent measurements.

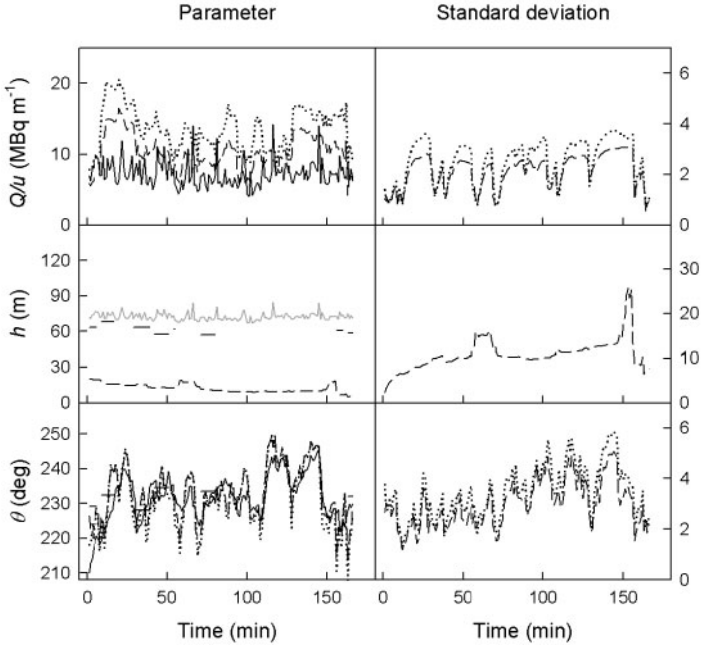

Figure 4. As Figure 3, results for Series 2. Solid horizontal lines in the h and θ plots (middle and lower left panels) show the plume Lidar scanning measurements.

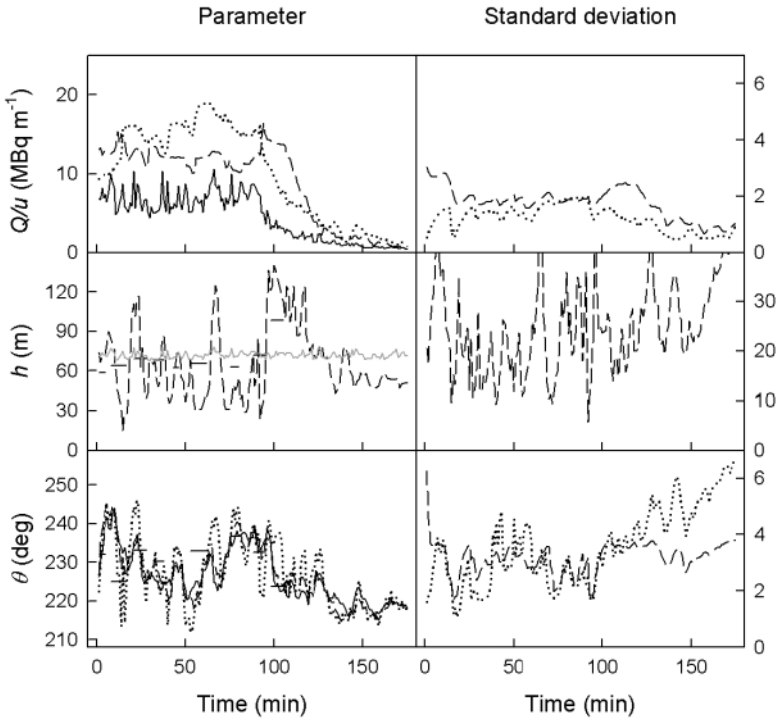

Figure 5. As Figure 4, results for Series 3.

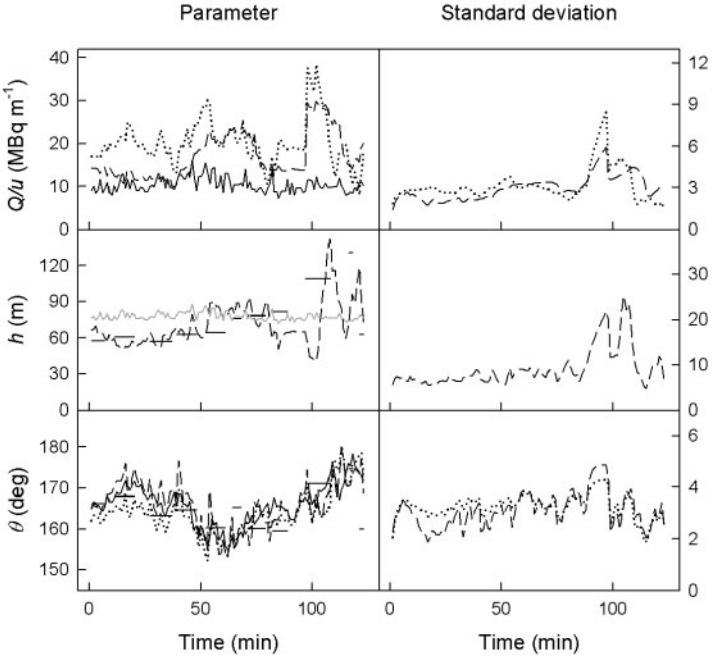

Figure 6. As Figure 4, results for Series 4.

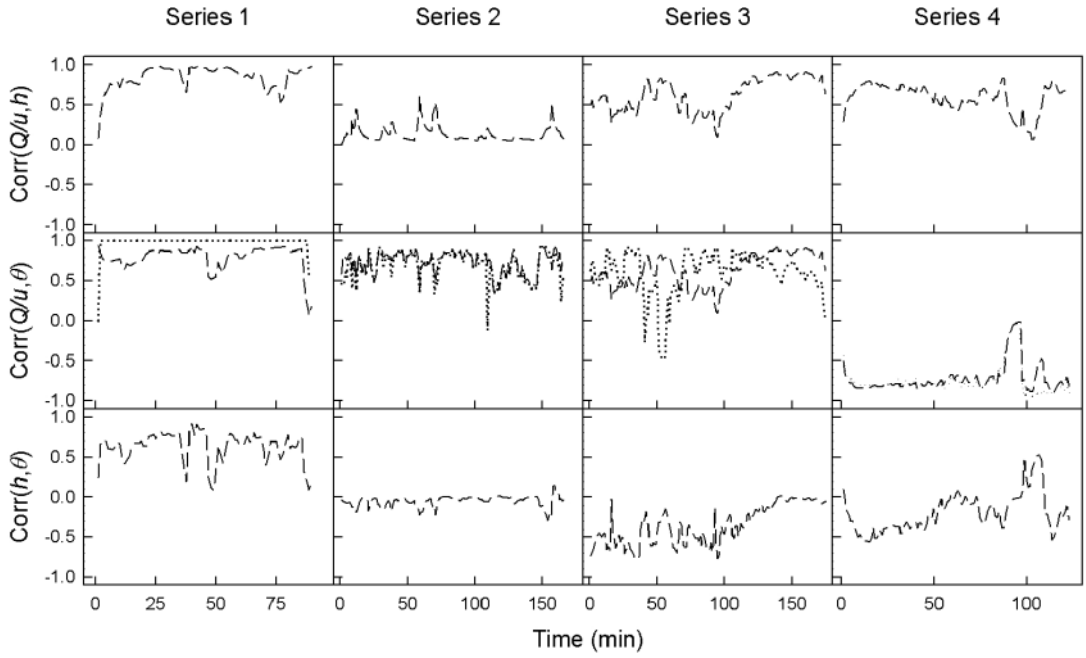

Figure 7. *A posteriori* parameter correlations obtained from $\Sigma^{xx}_{t|t}$. The dashed and dotted curves show the Kalman filter estimates obtained using Models I and II, respectively.

The estimated parameter correlations are shown in Figure 7. The strong correlation between the source term and the plume height is clearly recognised by the Kalman filter for three of the four time series. The small correlation found for Series 2 is linked to the poor estimate of the plume height, cf. Figure 4. The strong correlation between the source term and plume advection direction for all time series is due to the four detectors being placed on the same side of the plume centreline, cf. Figure 1; simulations, however, have shown this correlation to decrease when the detectors cover both sides of the plume[1]. Except for Series 1, where a moderate correlation is found, the Kalman filter estimates suggest little correlation between the height and the main advection direction.

More accurate source term estimates are expected from Model II. In this model, the free height parameter is replaced by the theoretical height. Overall, the theoretical plume height shown in Figures 4–6 appear to be a more accurate approximation to the Lidar measured height than the plume height derived from Model I. With the plume height given as an external forcing term (Model II), the estimated source term in the four time series is consistently found to exceed the measurements by approximately a factor of two. Similar estimates of the plume advection direction are obtained in the two models.

Figures 8 and 9 show the source term estimates $\dot{Q}/u$ provided by the Kalman filter versus the measured values for the two models, respectively. The straight lines are constrained linear regressions, $y = ax$, assuming no bias in the measurements of the release rate and the wind speed. Both models yield a ratio of estimated to measured source term of $\sim$1.8, however, with a significantly smaller spread in the case of Model II. Also, the data sets for the four time series have a larger overlap in Model II. This suggests that Model II gives a more accurate and robust estimate of the source term, provided a reliable value of the plume height is available.

Embedded parameters

In the proposed Kalman filter method, the embedded parameters of the state space model are determined by maximum likelihood estimation. The embedded parameters include the measurement error covariance R and the system error covariance Q.

Figure 10 shows the measurement error divided by the mean of the fluence rate for each of the four detectors, $\sqrt{R_{ii}}/\langle\varphi_i\rangle$, as a function of the downwind and cross-wind distances. The values are calculated independently for each of the four time series for both models. The measurement errors are seen to cluster around $\sqrt{R_{ii}}/\langle\varphi_i\rangle \approx 0.2$, with no clear trend observed as a function of x_0 or y_0. Preliminary studies indicate that the performance of the Kalman filter is not very sensitive to the values of the

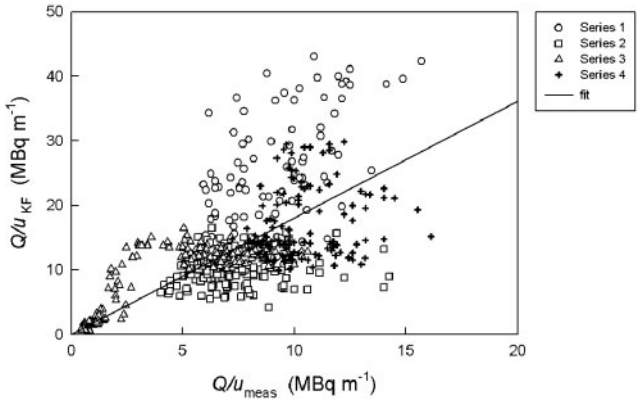

Figure 8. Scatterplot showing the estimated source term versus the measured source term using Model I. The straight line shows the constrained linear regression, $y = ax$. The least-squares estimate is $\hat{a} = 1.81$ ($R^2 = 0.84$).

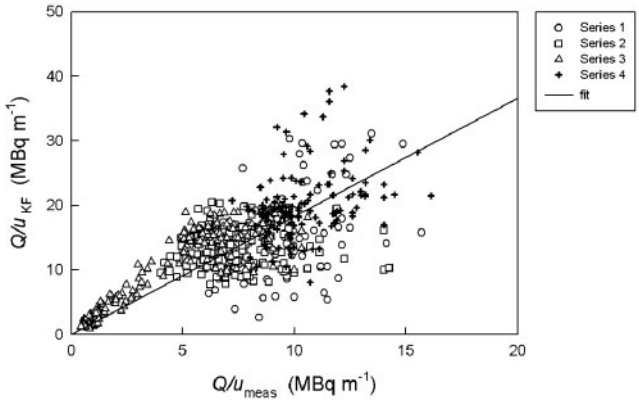

Figure 9. As Figure 8 using Model II. The straight line shows the constrained linear regression, $y = ax$. The least-squares estimate is $\hat{a} = 1.83$ ($R^2 = 0.91$).

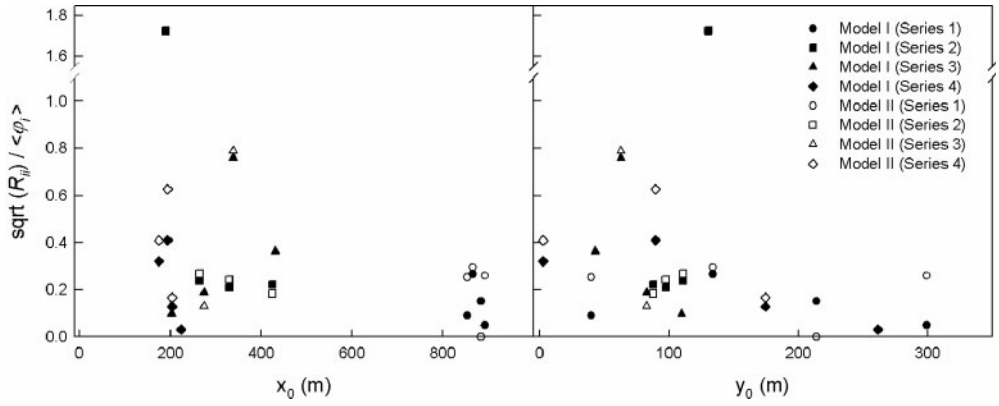

Figure 10. The estimated standard error $\sqrt{R_{ii}}$ for the fluence rate measurements divided by the mean fluence rate $\langle\varphi_i\rangle$ for each detector as a function of the down-wind (x_0) and cross wind (y_0) distances. When the difference between the results of the two models is less than a few percent, the points are indistinguishable.

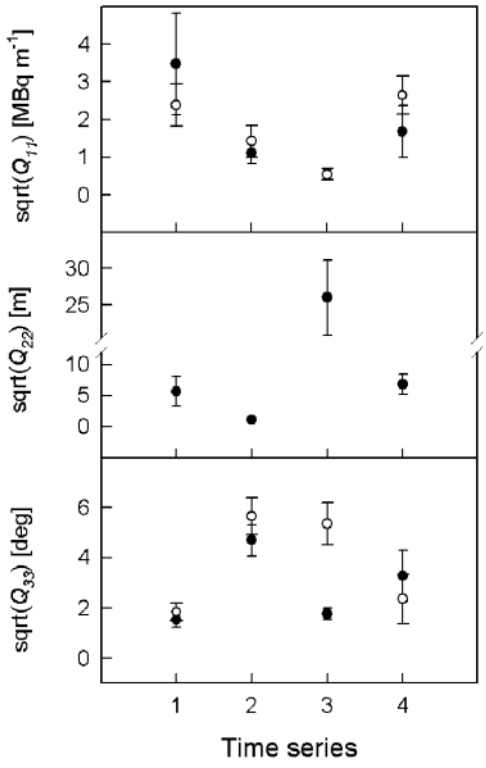

Figure 11. Square root of the diagonal elements of the system covariance matrix, $\sqrt{Q_{ii}}$, for the source term ($i = 1$), plume height ($i = 2$) and plume advection direction ($i = 3$). The solid and open circles show the results for Models I and II, respectively.

measurement error covariance. This suggests that it could be favourable in an operational context to exchange the maximum likelihood estimates $\sqrt{R_{ii}}$ by $c\bar{\varphi}_i$, where $\bar{\varphi}_i$ is an average over a few measurements and c is a constant factor ($c \approx 0.2$).

The diagonal elements of the Q matrix are shown in Figure 11. Q_{hh} is found to be almost zero for Series 2 in accordance with the height estimate shown in Figure 4 (middle left panel), which erroneously goes to zero. Likewise, the strong fluctuations exhibited by the plume height in Series 3 (Figure 5) is explained by Q_{hh} being substantially larger than in the other three cases.

WIND DIRECTION

The wind direction is measured from a local weather mast located at the SCK•CEN site and is in the preceding calculations included in the measurement vector. Owing to space–time variations in the local wind field, the measured wind could differ from the main plume advection direction. On the other hand, the Kalman filter is expected to compensate for such differences by assigning a large measurement error to these observed wind directions, thus relying more on the radiation measurements.

In the following, we extend the state space model to allow explicitly for a difference θ' between the observed wind direction and the plume advection direction. In the extended model, Model III, the state variables are $X_t^{\mathrm{T}} = \left(\dot{Q}/u, h, \theta, \theta'\right)_t$ while the observables are the same as in Models I and II. Unlike the first three state variables, the time evolution of θ' is assumed to be described by an autoregressive process of first order, that is, where the matrix A from Equation 14 is given by

$$A = \begin{pmatrix} 1 & 0 & 0 & 0 \\ 0 & 1 & 0 & 0 \\ 0 & 0 & 1 & 0 \\ 0 & 0 & 0 & a \end{pmatrix}. \tag{16}$$

The unknown parameter a is determined through the maximum likelihood procedure. The model prediction for the observed wind direction is

$$\theta_t^{\mathrm{w}} = \theta_t + \theta'_t. \tag{17}$$

Note that when θ' is equal to zero, the extended model reduces to Model I.

The Kalman filter results for Series 1 and 4 using Model III are shown in Figures 12–14. The parameter a for the two time series is estimated as 0.87 ± 0.14 and 1.01 ± 0.01, respectively. Thus, for both time series, the estimated value is consistent with $a = 1$, indicating a systematic deviation between the plume advection direction and the measured wind direction. Series 2 and 3 are not considered, as the detectors here are placed almost parallel to the plume advection direction, and hence the plume advection direction cannot accurately be determined from the fluence rate measurements alone.

The parameter estimates derived for Series 1 are shown in Figure 13. The Kalman filter estimate of θ' tends to zero, implying that the main plume advection direction is along the measured wind direction, cf. Equation 17, and that the parameter estimates of $\dot{Q}/u$, h, and θ are similar to those obtained previously (Figure 3). The results for Series 4 (Figure 14) indicate a larger deviation between the main plume advection direction and the measured wind direction. This implies that including the observed wind direction in the measurement vector of the previous models may have introduced a bias. We therefore in Figures 13 and 14 also show the results of a modified version of Model I, in which the wind direction has been omitted from the measurement vector, that is, $h^{\mathrm{T}} = (\varphi_1, \varphi_2, \varphi_3, \varphi_4)$. Generally, the parameter estimates in Model III are found

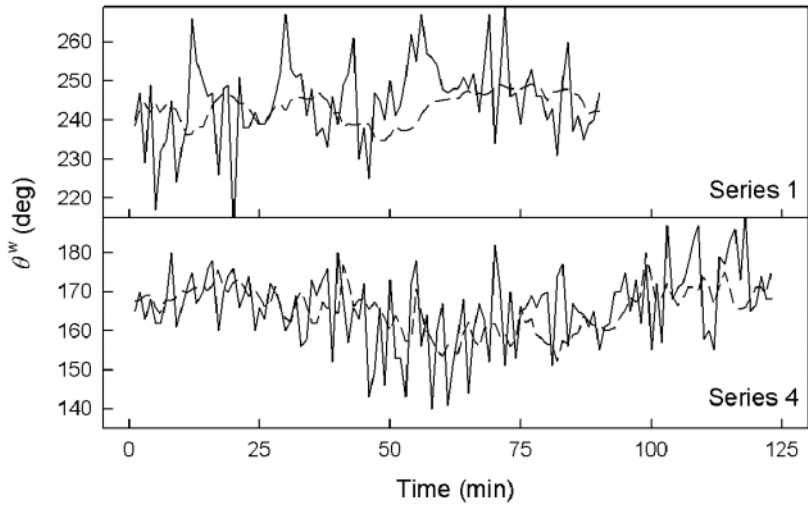

Figure 12. Kalman filter predictions for the observed wind direction, $\hat{\theta}^{w}_{t|t-1} = \hat{\theta}_{t|t-1} + \hat{\theta}'_{t|t-1}$, for Series 1 and 4 when using Model III (dashed curves). The solid curves show the measured values.

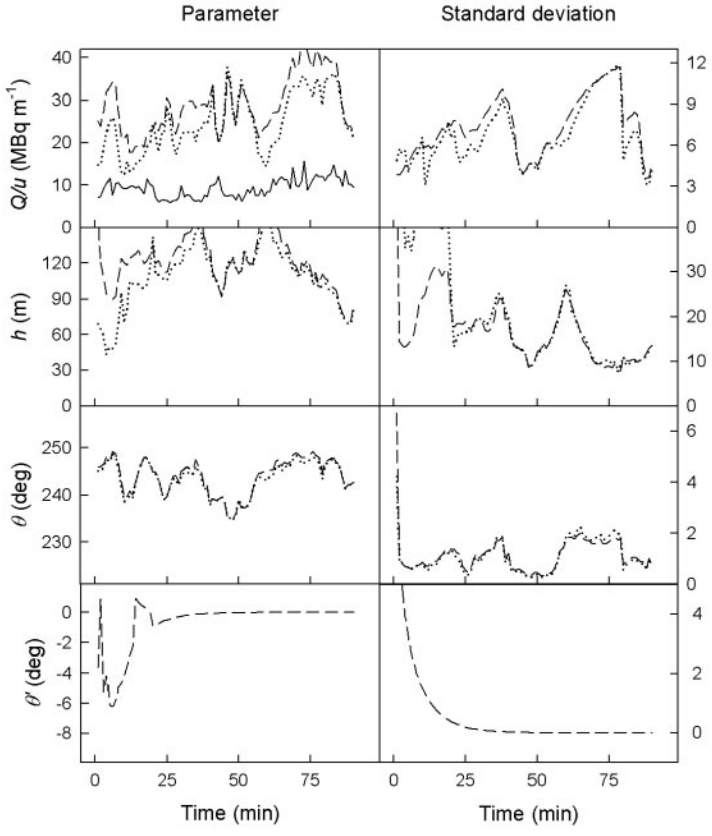

Figure 13. Filtered model parameters and associated standard deviations for Series 1. The dashed and dotted curves are the *a posteriori* Kalman filter estimates from Model III and the modified version of Model I, respectively, where the wind direction in the latter model is not included as an observable. Also shown is the measured source term (solid line).

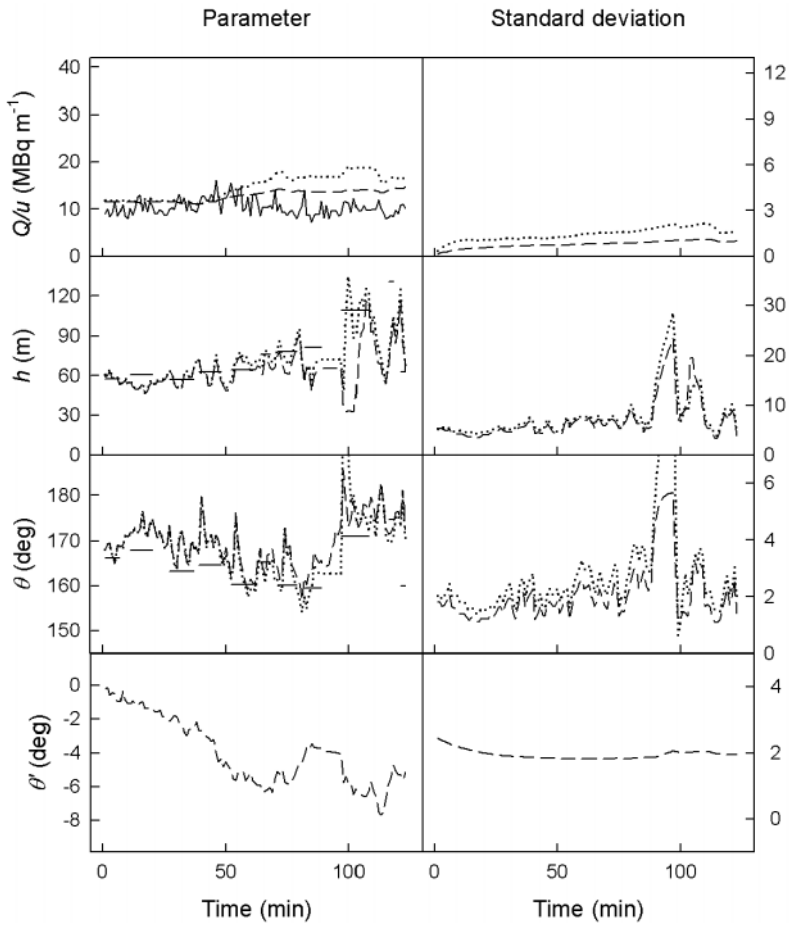

Figure 14. As Figure 13 for Series 4. Solid horizontal lines have been added in the h and θ plots that show direct plume measurements obtained from Lidar scanning.

to agree with the results obtained from this modified version of Model I.

This also follows from Figure 15, where the models are seen to yield similar results for θ'. For Series 1, the measured wind direction agrees with the plume advection direction. For Series 4 on the other hand, the Kalman filter finds a non-vanishing and time-varying θ', which peaks at (minus) 7–8°. Taking into account this effect, the source term estimates (Figure 14) are reduced compared to those of Model I (Figure 6), while the plume height remains unchanged.

Likelihood ratio test

Model III is effectively an extension of Model I, where the number of unknown, embedded parameters, dim(β), is increased from 14 to 18. When the extra parameters are set to zero, Model III reduces to Model I. To test whether or not these additional degrees of freedom may be statistically justified in terms of explaining the data, we use a likelihood ratio test[16]. Consider the hypothesis H_0: $\beta \in B_0$ (corresponding to Model I) against H_1: $\beta \in B \backslash B_0$ (corresponding to Model III), where B_0 is a subspace of the complete parameter space B. The likelihood ratio λ is defined by

$$\ln \lambda = \ln\left(\frac{L\left(\hat{\beta}_0\right)}{L\left(\hat{\beta}\right)}\right) = \ln L\left(\hat{\beta}_0\right) - \ln L\left(\hat{\beta}\right), \quad (18)$$

where $L(\hat{\beta}_0)$ and $L(\hat{\beta})$ are the maximum likelihood values corresponding to the optimal estimates of the parameters in Models I and III, respectively. Given the null hypothesis H_0 is true then

$$-2\ln \lambda \in \chi^2(\dim(\beta) - \dim(\beta_0)), \quad (19)$$

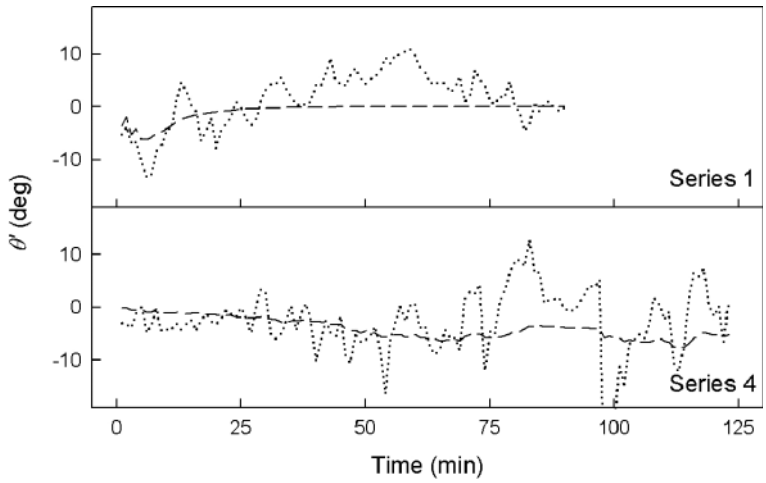

Figure 15. The difference between the measured wind direction and the main plume advection direction, $\theta'_t = \theta^{\mathrm{w}}_t - \theta_t$, for Series 1 and 4. The dashed lines are the Kalman filter estimates from Model III. The dotted lines show $\theta^{w}_t - \hat{\theta}_{t|t}$ obtained from the modified version of Model I, where the wind direction is not included as a direct observation, and the measured wind direction θ^{w}_t has been exponentially smoothened.

Table 3. Likelihood ratio test comparing Model I ($\dim(\beta_0) = 14$) and Model III ($\dim(\beta) = 18$).

	Test	
	$-2\ln\lambda$	Inverse χ^2
Series 1	5.5	0.24
Series 4	28.3	1.07×10^{-5}

that is $-2\ln\lambda$ belongs to a χ^2-distribution with degrees of freedom given by the difference in the number of unknown parameters. A small value ($\ll 1$) of the inverse χ^2 implies that we must reject the null hypothesis H_0.

Table 3 shows the results of comparing Models I and III using the likelihood ratio test. For Series 4 the extension of Model I seems to be justified, since the inverse $\chi^2 \approx 0$, but not for Series 1, where the inverse $\chi^2 \approx 0.24$. This is in accordance with the Kalman filter results, where the parameter estimates from the two models are seen to change noticeably for Series 4 but not for Series 1. Note that the modified version of Model I, which does not including the wind direction as an observable, cannot be compared to any of the other models, since the likelihood ratio test demands that the models are tested on the same data. However, since the Kalman filter results for this model are similar to those of Model III, the modified version of Model I should arguably be justifiable as well when compared to the original Model I.

DISCUSSION

A main problem in facilitating operational use of the Kalman filter method, that is, in the context of nuclear emergency management, lies in tuning the system and measurement error covariance matrices Q_t and R_t, which along with additional embedded parameters must either be provided externally or estimated from data. In the present study, Q_t and R_t are assumed to be constant, diagonal matrices, and maximum likelihood estimates of the embedded parameters are obtained using the full range of the data.

The model, however, may readily be extended to include both time-dependent and non-diagonal error covariance matrices. The results obtained indicate that the measurement standard errors to a first order approximation should be proportional to the mean fluence rate, $\sqrt{R_{ii}} = c\bar{\phi}_i$, cf. Figure 10. Since in the general case the radiation field changes over time, for example, due to changes in the radionuclide release rate or in the mean advection direction, the measurement error covariances should also be time-dependent to account for such changes. Non-diagonal matrix elements naturally arise when allowing for systematic measurement errors, considering that the measurement error covariance matrix R_t includes not only measurement noise but also model and completeness error, for example, errors due to un-modelled dynamics.

The same holds for the system error covariance Q_t controlling the temporal variation of the state vector. One might expect the plume dispersion parameter covariances both to exhibit strong

correlations and to be time-dependent, since these parameters will be affected by, for example, variations in the atmospheric turbulence.

In an on-line automatic system used for decision support it is essential that calculations can be carried out between time updates. For the present study, calculations were performed on a SunFire 3800 with 1200 MHz UltraSparc III processors. Using a partially optimised numerical code, maximum likelihood estimation for each of four time series required a few minutes of computer time for Model II (11 parameters) and 10–15 min for Model III (18 parameters).

For fast computing, one may rely on (partly) predefined parameters β, assuming that these are close to the optimal values, that is, the maximum likelihood estimates. Such a set of parameters could be determined from expert judgments and/or measurements. Another possibility is to use an empirical Bayesian approach, where prior knowledge about the parameters is expressed using prior distributions. As soon as local observations become available, information about the parameters are updated using a maximum a posteriori (MAP) method[17].

Considering longer time-series, that is, for a prolonged release, it may be advantageous periodically to re-estimate the embedded parameters, since the parameter values that optimise the likelihood function for a subset of observations need not be optimal for the complete time series. Conversely, if for instance the meteorological conditions or the radionuclide composition change during the release, the embedded parameters should be re-assessed to reflect such changes. In this case, only the most recent part of the time series should be used for estimating the parameters.

To account for realistic accident scenarios, the simple gaussian plume model should be amended to include the simultaneous release and decay of many different radionuclides and should also be supplemented by models for dry and wet deposition. While such extensions are straightforward, the detailed treatment depends on the measurements assumed available. If only gamma dose rates or gross count rates are measured, the radionuclide composition of the release becomes unobservable. Still, the method can be used to assess the total activity released, if the radionuclide makeup of the plume is assumed known.

The state space method is very flexible and may be extended to accommodate a more detailed physical description of the various processes giving rise to the radiation field. If the dynamics of the release and atmospheric dispersion can be described by ordinary linear differential equations, an autoregressive stochastic model should be substituted for the present simple random walk model. Also non-linear models can be formulated in the state space formalism[18]. We have implicitly assumed up to now that simultaneous measurements are performed at equidistant time points. If this is not the case, however, the state space model can be formulated as a continuous time system, allowing incorporating irregular or asynchronous measurements[6].

Finally, for retrospective data processing the proposed state space model constitutes an equally appropriate framework. In this case, rather than using a filtering procedure, the state variables should be determined from a Kalman Smoother[4], for which each state vector estimate is based on all data in the series. The embedded parameters may also in this case be obtained by maximum likelihood estimation.

CONCLUSIONS

In the present study we have analysed a Kalman filter method for the estimation of atmospheric release of radionuclides from a nuclear research reactor using a set of experimental radiation monitoring data. The method has been analysed for three different state space models.

The Kalman filter method is in general found to provide good estimates of the gaussian plume model parameters, that is, the source term (the emission rate divided by wind speed), plume height and advection direction, when the ground-based radiation measurements span the plume in the cross-wind direction. For a less optimal detector placement it proves difficult to resolve variations in the plume height and source term. The proposed method, however, still provides consistent estimates of the parameters while associated with large prediction errors.

Numerical estimates of the source term are found consistently to exceed the measured values by approximately a factor of 1.8. A similar discrepancy between measured and calculated values has previously been observed in deterministic calculations with the Rimpuff atmospheric dispersion model, used in EU decision support systems[19]. In these calculations, where the input data are the measured source term and a theoretical plume height, the fluence rates are found to exceed the measured values by up to approximately a factor of two[20].

When including the wind direction as an observable, results indicate that improved Kalman filter estimates may be obtained by adopting an extended state space model, Model III, which allows explicitly for a difference between the measured wind direction and the main plume advection direction. This is also supported by a likelihood ratio test. Alternatively, one might exclude wind direction measurements from the input data by using the simpler Model I. To infer accurate estimates of the plume advection direction from ground-based radiation measurements only, however, these measurements must span the plume in the cross-wind direction. For

some of the data series examined, for example, Series 2 and 3, the detector placement was not optimal and excluding wind direction measurements for these time series rendered the calculations unstable.

Overall, this numerical study suggests that the Kalman filter method could be a valuable operational tool for estimating the release and atmospheric dispersion during an atmospheric release of radionuclides. Essentially, the Kalman filter is a recursive estimator, which allows updated estimates of state parameters to be calculated as soon as new data become available. Based on on-line radiological and meteorological observations the filtering procedure thus allows efficient inference of atmospheric dispersion parameters including the radionuclide source term.

The proposed state space model constitutes a flexible framework that accommodates both the inclusion of input data obtained from a variety of measurements and being of irregular time sequences as well as the extension of the method to more elaborate models for the dispersion and deposition of radionuclides.

REFERENCES

1. Drews, M., Lauritzen, B., Madsen, H. and Smith, J. Q. *Kalman filtration of radiation monitoring data from atmospheric dispersion of radioactive materials*. Radiat. Prot. Dosim. **111**(3), 257–269 (2004).
2. Rojas-Palma, C. *et al. Experimental evaluation of gamma fluence-rate predictions from ^{41}Argon releases to the atmosphere over a nuclear research reactor site*. Radiat. Prot. Dosim. **108**(2), 161–168 (2004).
3. Kalman, R. E. *A new approach to linear filtering and prediction problems*. Trans. ASME – J. Basic Eng. D **82**, 35–45 (1960).
4. Shumway, R. H. *Applied statistical time series analysis*. (London: Prentice-Hall) (1988).
5. Jazwinsky, A. *Stochastic Processes and Filtering Theory*. (New York: Academic Press) (1970).
6. Kristensen, N. R., Madsen, H. and Jørgensen, S. B. *Parameter estimation in stochastic grey-box models*. Automatica **40**, 225–237 (2004).
7. Madsen, K. and Tingleff, O. *Robust subroutines for non-linear optimization*. Report NI-90-06, Technical University of Denmark (1990).
8. Gorshkov, V. E., Karmazin, I. P. and Tarasov, V. I. *Reduced integral solutions for gamma absorbed dose from Gaussian plume*. Health Phys. **69**(2), 210–218 (1995).
9. Drews, M., Aage, H. K., Bargholz, K., Jørgensen, H., Korsbech, U., Lauritzen, B., Mikkelsen, T., Rojas-Palma, C. and Van Ammel, R. *Measurements of plume geometry and argon-41 radiation field at the BR1 reactor in Mol*, Belgium. NKS-**55** (2002).
10. Lauritzen, B. *Nuclear emergency preparedness. Final report of the Nordic Nuclear Safety Research project BOK-1*. NKS-**63**, (2002).
11. Jørgensen, H. E. and Mikkelsen, T. *Lidar measurements of plume statistics*. Boundary-Layer Meteorol. **62**, 361–378 (1993).
12. Jørgensen, H. E., Mikkelsen, T., Streicher, J., Herrmann, H., Werner, C. and Lyck, E. *Lidar calibration experiments*. Appl. Phys. B **64**, 355–361 (1997).
13. Seinfeld, J. H. *Atmospheric Chemistry and Physics of Air Pollution*, (John Wiley & Sons) (1986).
14. Bultynck, H. and Malet, L. *Evaluation of atmospheric dilution factors for effluents diffused from an elevated continuous source*, TELLUS **24**, 455–472 (1972).
15. Gifford, F. A. *Turbulent diffusion typing schemes: A review*. Nucl. Safety **17**, 25 (1976).
16. Rao, C. *Linear Statistical Interference and its Applications*. (New York: John Wiley & Sons) (1973).
17. Goodwin, G. C. and Payne, R. L. *Dynamic System Identification: Experiment Design and Data Analysis*. (New York: Academic Press) (1977).
18. Ljung, L. and Söderström, T. *Theory and Practice of Recursive Identification* (Cambridge, MA: MIT Press) (1983).
19. Ehrhardt, J. *RODOS—Decision support system for off-site emergency management in Europe*. European Commission EUR-Report 19144 EN (2000).
20. Lauritzen, B. *et al. Atmospheric dispersion of radioactive releases from a nuclear research reactor: Measurements and modelling of plume geometry and gamma radiation field*. In: Proceedings of the 8th International Conference on Harmonisation within Atmospheric Dispersion Modelling for Regulatory Purposes, Sofia, Bulgaria. Batchvarova, E. and Syrakov, D., Eds. (2002).